Development of the Viking Parachute Configuration by Wind-Tunnel Investigation

SY STEINBERG*
Martin Marietta Corporation, Denver, Colo.
PAUL M. SIEMERS, III†
NASA Langley Research Center, Hampton, Va.
AND
ROBERT G. SLAYMAN‡
Goodyear Aerospace Corporation, Akron, Ohio

Several experimental investigations to obtain the drag performance of 10% scale-model disk-gap-band-type parachute assemblies trailing in the Viking forebody wake were conducted over the range of Mach 0.2 to 2.6. The wind-tunnel tests varied both the canopy trailing distance and ratio of suspension line length to canopy diameter. The data obtained permitted optimization of both parameters. Parachute drag performance in the forebody wake is markedly degraded transonically beginning at $M \approx 0.6$, reaching a minimum value at $M = 1.0$, then approaching the subsonic value for the selected configuration as Mach number is increased to 1.4. Further increase in Mach number causes the drag coefficient to again decline. A 20% increase in parachute-alone transonic drag coefficient was obtained by increasing suspension-line length ratio (S/D_o) from 1.16 to 1.73. Increasing canopy trailing distance also significantly improved drag performance. Flight-test and wind-tunnel data are in good agreement.

Nomenclature

A = aeroshell forebody
BC = base cover
C_{D_p} = parachute drag coefficient (drag force/$q_\infty S_o$)
d = maximum forebody diameter (13.8 in.)
D_o = parachute nominal diameter (5.3 ft)
DGB = disk-gap-band-type canopy
L = Lander configuration
M_∞ = freestream Mach number
P_o = reservoir or total pressure, lb/ft^2
q_∞ = freestream dynamic pressure, lb/ft^2
R = riser length (between bridle and suspension line confluence)
Re_d = Reynolds number based on $d(Vd\rho/\mu)$
S = suspension-line length, ft
S_o = parachute reference area (22.06 ft^2)
V = freestream velocity, fps
VLC = Viking Lander Capsule
x = canopy axial trailing distance behind forebody, ft
α = forebody angle of attack, deg
ρ = freestream air density, slug/ft^3
μ = viscosity coefficient, lb-sec/ft^2

Introduction

PRELIMINARY design studies for the Viking Lander Capsule (VLC) established the requirement for an aerodynamic decelerator subsystem during one phase of the Mars entry trajectory. The subsystem consists of a main parachute assembly that is deployed by a mortar from a canister in the vehicle base cover. Mortar firing is initiated by a radar altimeter signal at an altitude of 25,400 ft above the surface. Accordingly, the particular Mars atmosphere[1] encountered determines the environment and conditions for parachute deployment. These conditions vary from $M_\infty = 0.75$ to 2.20 at dynamic pressures ranging from $q_\infty = 6.27$ to 9.26 lb/ft^2. After aeroshell separation (A from VLC), 7 sec after mortar fire, the vehicle remains suspended on the parachute, trailing in the wake of the blunt forebody payload (L + BC), until the multinozzle terminal descent engines are ignited and the parachute base cover elements are staged from the Lander. The parachute flight phase terminates at a system velocity ranging from about $V = 89$–231 fps.

The parachute configuration preliminary design, which consisted of a disk-gap-band-type (DGB) canopy, evolved primarily on the basis of both pre-Viking flight test programs[2–4] and scale-model wind tunnel tests[5–7] sponsored by NASA and the Air Force. The 10% scale-model arrangement, presented schematically in Fig. 1, including the tabulated geometric properties, was the basis for several series of wind-tunnel investigations[8,9] to obtain the required parachute drag performance throughout the anticipated Mach number range. These tests, conducted in the Arnold Engineering Development Center (AEDC) PWT 16T and 16S facilities and the NASA Langley Research Center 16-ft Transonic Dynamics Tunnel, included variation of parachute trailing distance (x/d), suspension-line length ratio (S/D_o) and riser line length (R).

In addition to wind-tunnel tests, some water-table investigations were performed to establish the interdependence (in two dimensions) of the two-body system and the interference flowfield as a function of canopy trailing distance. This paper summarizes the important details of the investigations including model(s), description(s), instrumentation used, test environment, and test technique. It chronologically traces the results leading to the final selected configuration for Earth atmosphere flight qualification tests.

Apparatus

Test Facilities

Descriptions of the wind tunnels are available from test facility handbooks[10,11] and, for brevity, are omitted here. The

Presented as Paper 73-454 at the AIAA 4th Aerodynamic Deceleration Systems Conference, Palm Springs, Calif., May 21–23, 1973; submitted September 4, 1973; revision received October 15, 1973. Work performed under Contract NAS1-9000, managed by NASA-Langley Research Center, Viking Project Office, Hampton, Va.

Index categories: Jets, Wakes, and Viscid-Inviscid Flow Interactions; Subsonic and Transonic Flow; Entry Deceleration Systems and Flight Mechanics (e.g., Parachutes).

* Senior Group Engineer, System Analysis Department. Associate Fellow AIAA.

† Aerospace Technologist, Viking Project Office.

‡ Formerly Project Engineer, Viking Decelerator. Deceased November 29, 1973.

GEOMETRIC PROPERTIES OF PARACHUTE

Item	Relative Value	Value
Nominal Diameter	D_o	5.3 ft
Total Area, S_o*	$\pi D_o^2/4$	22.06 ft^2
Geometric Porosity**	0.125 S_o	2.76 ft^2
Disk Area***	0.53 S_o	11.69 ft^2
Disk Diameter	0.726 D_o	3.85 ft
Gap Area	0.12 S_o	2.65 ft^2
Gap Width	0.042 D_o	0.223 ft
Band Area	0.35 S_o	7.72 ft^2
Band Width	0.121 D_o	0.641 ft
Vent Area	0.005 S_o	0.110 ft^2
Vent Diameter	0.07 D_o	0.371 ft
Number of Suspension Lines	---	48
Thickness of Suspension Lines	0.00011 D_o(FS)	0.07 in.
Thickness of Suspension Lines Actually Tested	0.00157 D_o(Model)†	0.100 in.
Suspension Line Lenghts (S)	1.00 D_o	5.300 ft
	1.16 D_o	6.148 ft
	1.52 D_o	8.056 ft
	1.73 D_o	9.169 ft
	1.85 D_o	9.805 ft
	2.26 D_o	11.980 ft

*Disk + gap + band.
**Gap + vent provide 12.5% geometric porosity.
***Includes vent.
†Based on wide edge dimension.

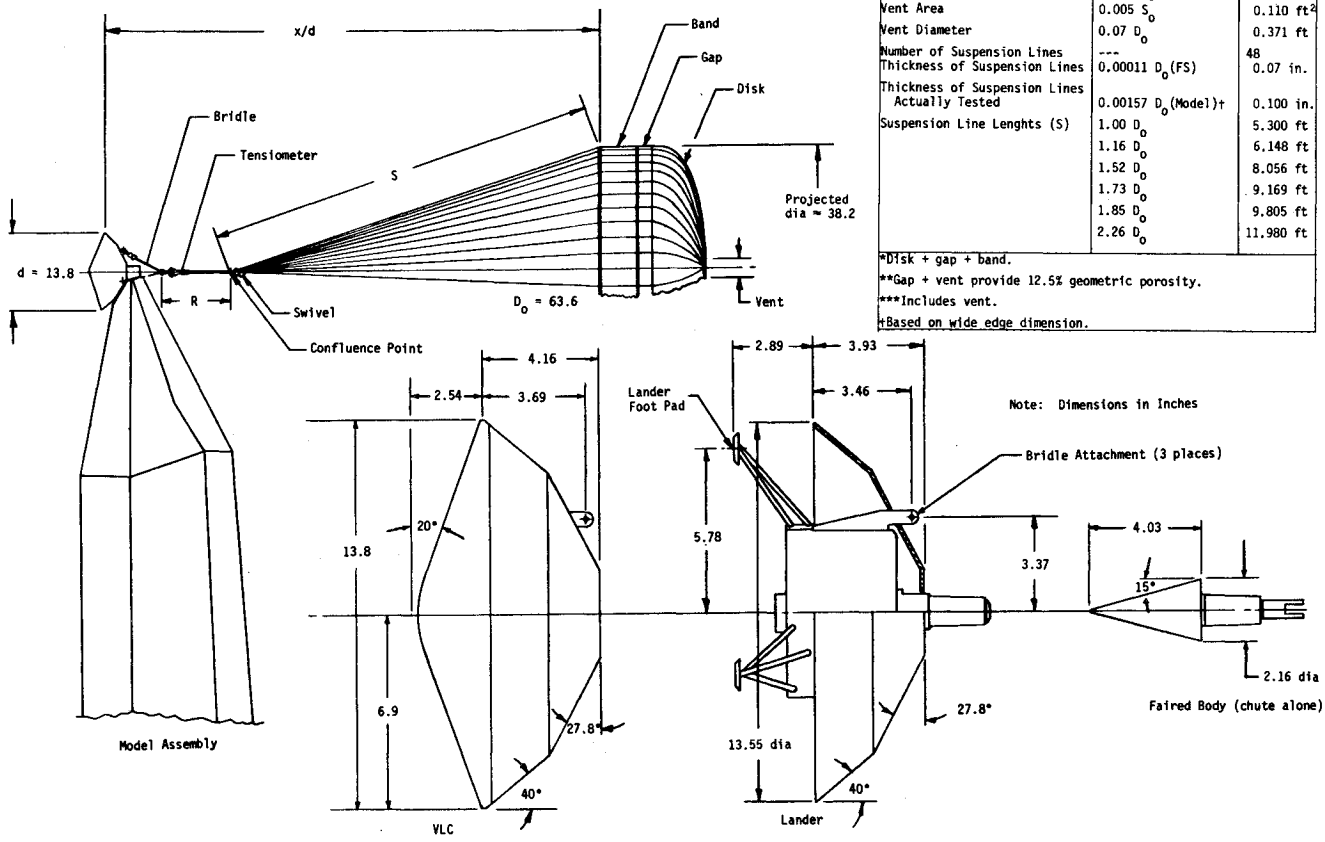

Fig. 1 Ten-percent model configuration.

6-ft water table is shown in Fig. 2. The table was borrowed from the Univ. of Colorado at Boulder. The flow conditions are determined by calculating the Froude number along the nozzle contour centerline; this is then equated to the Mach number in airflow. The water-table investigation simulated a tunnel Mach number range from $M \approx 0.40$ to $M \approx 1.30$ at the forebody position. The parachute canopy was placed at various axial positions downstream of the forebody.

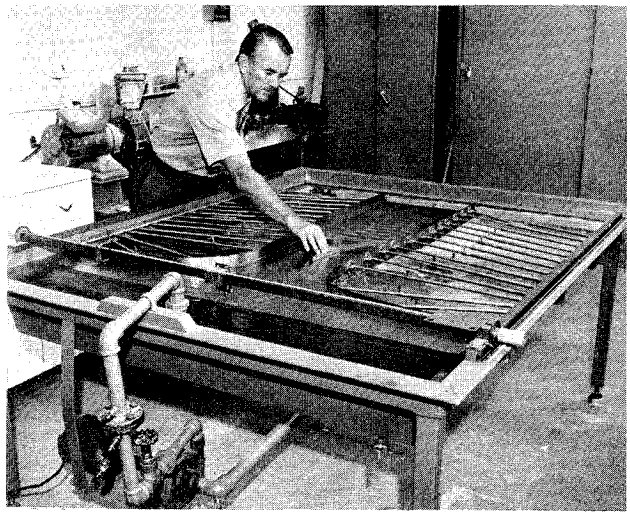

Fig. 2 Water-table arrangement for flowfield studies.

Models and Instrumentation

10% forebodies

These rigid-body models consisted either of the VLC entry vehicle or the Lander and base cover (L+BC), and are dimensionally shown in Fig. 1. Model components were primarily constructed of aluminum and steel. The internal model structure of the VLC configuration comprised two sets of flexure assemblies[12] supporting a centerbody, which houses the load cells used for axial load measurements. The flexures transmitted axial load to the load cells while resisting lateral loads and moments caused by parachute motion in the tunnel. The L+BC model used the centerbody assembly fitted with a cover representing the outer geometry of the Lander box structure, including a simulation of the protruding support legs. Either body could be secured to the vertical support strut assembly by a short sting. For parachute-alone tests, a separate sting with a 30° included-angle conical fairing secured the assembly to the vertical strut, as shown in Fig. 1.

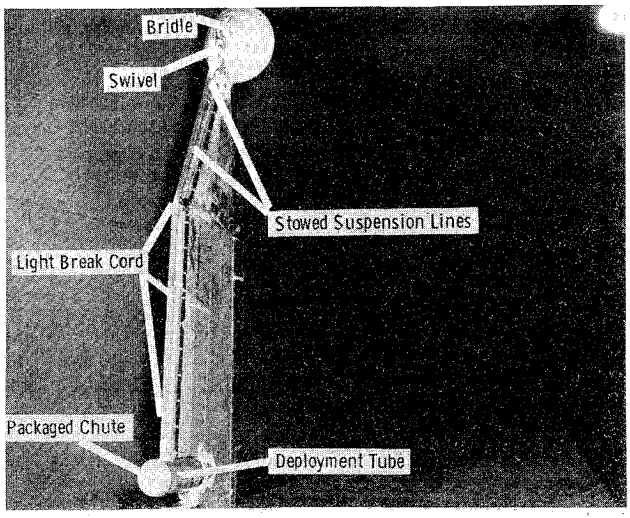

Fig. 3 Model installation in AEDC PWT 16S facility.

Parachute Models

All the 10% parachute models used for the tests were disk-gap-band type designed and fabricated by Goodyear Aerospace Corp. They were designed to withstand extended periods of testing at dynamic pressures up to 100 lb/ft^2 and Mach numbers to 2.6, with possible retest capabilities. The major non-dimensional physical parameters of the parachutes are tabulated in Fig. 1. Most of the models were designed with a geometric porosity of 12.5%; 13% geometric porosity was provided on two models by increasing the vent diameter.

Although the test models geometrically represent a 10% scale model of the flight article, all physical characteristics such as suspension-line diameter, canopy cloth thickness, circumferential tape size, and over-all parachute relative stiffness, were not accurately scaled due to physical limitations and test operation constraints.

The canopy gores were fabricated from Dacron 52 rip-stop cloth with a minimum strength of 100 lb/in. in both the warp and fill directions, with a weight of 2.1 oz/yd^2. Cloth porosity was approximately 128 ft^3/min. The various tapes, sewing threads, webbings, and suspension lines were made of either Nylon or Dacron.

Standard parachute fabricating techniques were used to construct the models, with particular attention to dimensional accuracy. Size limitations prevented model duplication of many construction details used in the actual flight article. As an example, disk gore panels were cut double width so that only 24 panels were required to fabricate 48 disk gores. The 48-band gores were fabricated from three panels. Other variations related primarily to sewing patterns, types of stitching, etc., and did not compromise model performance.

Canopy trailing distance with respect to the forebody was varied by alternating the suspension line lengths of the models and/or varying the riser and bridle lengths. Suspension lines were attached to a confluence ring in four groups of six. The ring was attached to a special swivel adapted to the forebody model.

Water-Table Models

These two-dimensional models were made to scales of 0.013 and 0.0065. The forebody models were made from metal blocks, while the simulated inflated canopy models were made from brass sheet shaped in accordance with measurements made from inflated canopy photographs obtained during wind-tunnel tests.

Test Instrumentation

The 10% scale-model instrumentation consisted of load cells and a tensiometer for measuring axial loads, motion-picture cameras for recording parachute oscillations and canopy shape, and thermocouples for measurement of forebody temperature. The load cells in the VLC configuration were Baldwin-Lima-Hamilton (BLH) C2M1 miniature cells of 500 and 2000 lb capacities. The lower capacity cell measured forebody load, and the other load cell measured total parachute and forebody combined load. Only the larger capacity load cell was used during tests with the L+BC configuration. Forebody temperature was monitored using iron-constantan thermocouples to provide a bias correction to the load-cell readings due to model temperature changes. The tensiometer was used as a redundant system for obtaining parachute axial load during runs with the Viking forebody in place and as the sole measurement system for parachute-alone runs.

The water-table tests employed a 4 × 5-in. Graflex camera for still photographs.

Test Environment and Procedure

Test Conditions

Table 1 chronologically lists the test runs made in each facility, including forebody configuration and geometric properties of the parachute. Also listed are both the approximate Mach number and the dynamic pressure ranges for each test. With the exception of the initial two-test series, test dynamic pressure was $q_\infty \approx 80$ lb/ft^2; for the first two-test series the test dynamic pressure environment was varied from about 5 lb/ft^2 to a maximum of about 100 lb/ft^2.

Table 1 Test run program

Facility	Date	Forebody	x/d	S/D_o	M_∞	q_∞ (lb/ft^2)
AEDC PWT 16T	2/71	VLC	5.35	1.0	0.20–0.65	Low–100
			6.26	1.16		
			↓	1.0		
		None	0	↓	0.60–1.40	100
		↓	↓	1.16[a]	↓	↓
NASA LRC 16 TDT	4/71	None	0	1.16	0.40–0.85	Low–100
		VLC	6.12	↓	0.27–0.85	
			↓		↓	
			5.46	1.0	0.45–0.93	
			6.12	1.16[a]	0.27–0.85	
			9.00	1.16	0.30–0.95	
			6.79	1.3	0.60–0.95	
AEDC PWT 16T	6–7/71	VLC	9.16	1.85	0.80–1.40	55–81
			7.62	1.52	0.52–1.35	73–85
			11.02	2.26	0.50–1.37	80
			9.14	1.16	0.20–1.40	67–80
		L+BC	9.16	1.85		55–81
			7.62	1.52		56–82
			6.40	1.16	0.20–1.37	57–80
			11.02	2.26	0.20–1.40	60–80
			8.53	1.73		60–81
		None	0	1.85		58–80
		↓	0	1.73	↓	60–81
AEDC PWT 16S	8/71	VLC	6.50	1.16	1.8–2.20	78–81
↓	↓	↓	8.53	1.73	1.8–2.60	70–79

[a] All parachute canopies have total geometric porosity 12.5% except those marked with a superscript, which are 13.0%.

Test Procedure

During the first two investigations at the AEDC-PWT and NASA-LRC facilities, the parachute was rigged in an extended position before tunnel start-up. At PWT 16T, it was draped behind the strut; at the 16-ft TDT it was extended behind the support strut and tethered with light break cord from the canopy crown to the sting support strut. Data were usually obtained at selected test conditions as Mach number was increased; some data were also recorded at randomly selected points while M_∞ or P_o were adjusted.

The test procedure pursued during the remaining investigations differed from that described previously in that the parachute was pneumatically deployed after reaching the desired test condition.[8] Figure 3 is a photograph of the installation in the AEDC PWT 16S facility, with the parachute packaged in the

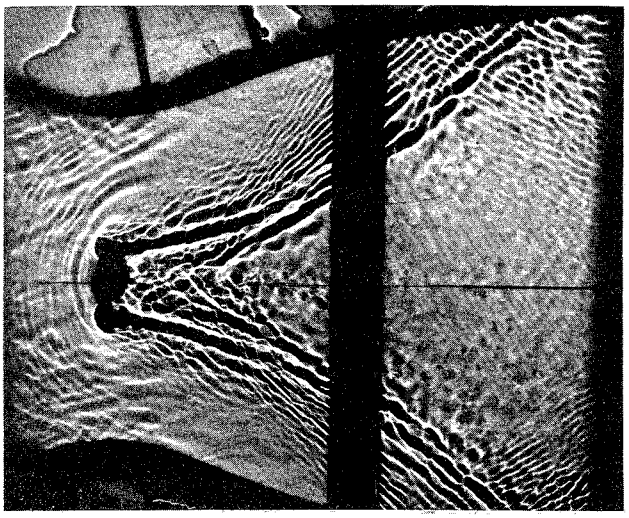

Fig. 4a Forebody results, $M \approx 1.4$.

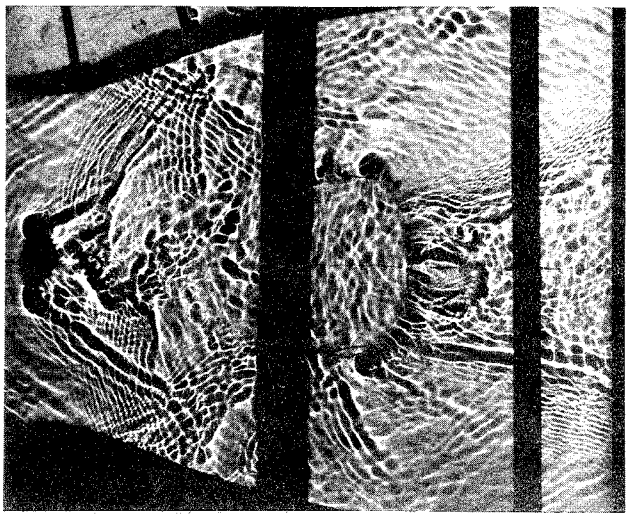

Fig. 5a Results with canopy behind VLC; $x/d = 5.0$.

deployment tube. Normally, the parachute was deployed at the highest test Mach number and data were obtained as Mach number was decreased. During these test series, data were also recorded while test Mach number was being changed.

Discussion of Results

Forebody—Canopy Flowfield Interference

During the first test series[12] at the AEDC PWT 16T facility (2/71), successive failures of the parachute suspension lines were experienced, with the canopy trailing behind the VLC forebody at $x/d = 5.35$ and 6.26 ($S/D_o = 1.0$ and 1.16). The failures occurred in the confluence region and were attributed to severe vibration of the suspension lines and resulting friction between the Nylon fabric and metal fitting adapting the parachute to the riser, swivel, and bridle. The sparse data obtained before noting the suspension-line failures with the TV monitor provided evidence of severe drag-coefficient degradations beginning at $M \approx 0.55$. Two parachute-alone runs were successfully completed over the Mach number range from $M = 0.6$ to $M = 1.4$ without an accompanying drag-coefficient degradation. It was therefore concluded that the wake environment behind the VLC forebody caused both the intolerable drag reductions and the severe suspension-line vibration and canopy oscillation. Accordingly, a test program using a water table was implemented to qualitatively study the mutually interfering flowfield between the forebody and parachute canopy as a function of canopy trailing distance. Figures 4 and 5 summarize the water-table results, with visual representations of both individual and two-body interference flowfields. Figures 4a and 4b show the independent flowfields involving the VLC and nominal basic canopy, respectively, at a simulated Mach number (Froude analogy) of about 1.4. The interfering body flowfields are shown in Figs. 5a and 5b for canopy positions of $x/d = 5.0$ and 8.0, respectively. The difference between the canopy positions is evident in that the flowfield for the canopy at the shorter trailing distance bears no resemblance to either independent flowfield given in Fig. 4; at $x/d = 8.0$, however, there is a resemblance to both model-alone photographs in that there is little distortion of the interference flowfield, as can be seen by comparing Fig. 4b with Figs. 5a and 5b. This evidence of two-body induced interference at close separation distances will be reflected in the quantitative results obtained in the wind tunnel.

Wind-Tunnel Tests (NASA/LRC 16-ft TDT Series)

After experiencing the parachute system suspension-line failures and drag-coefficient degradation trends during the initial test series at AEDC PWT 16T, it was necessary to modify the

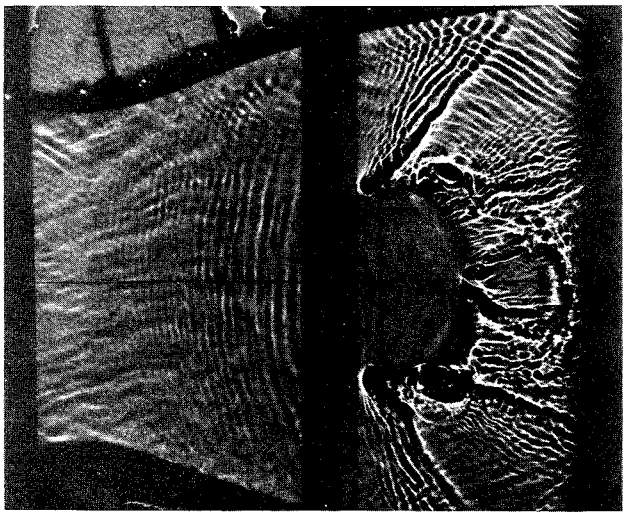

Fig. 4b Canopy-alone results, $M \approx 1.4$.

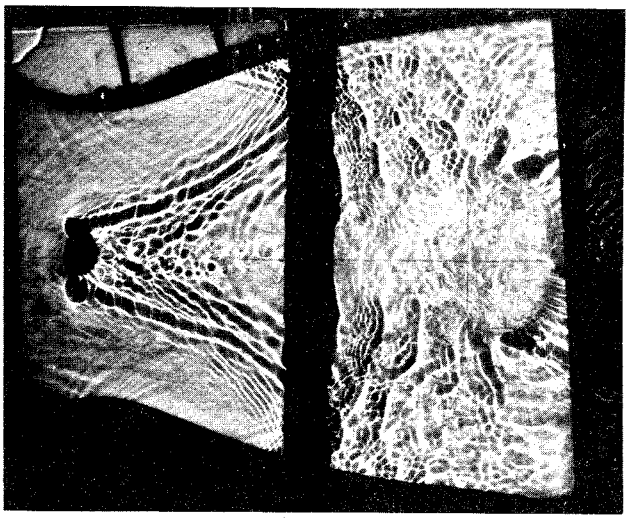

Fig. 5b Results with canopy behind VLC; $x/d = 8.0$.

suspension-line confluence end arrangement to eliminate the failures while obtaining additional transonic performance data in the forebody wake environment. The test series at the 16-ft TDT accomplished these goals in that the large drag reductions were verified and the model parachute configurations did not fail, although failure of some of the test-peculiar hardware (swivel and fabric riser) did occur. These results are summarized in Fig. 6, which presents parachute drag coefficient as a function of Mach number for several canopy trailing distances and parachute suspension-line lengths. Also included is a chute-alone run from the initial test series at AEDC. It is evident that drag coefficient increases as a function of trailing distance, and, at $x/d = 9.0$, the subsonic C_{D_p} is very nearly equivalent to the chute-alone value. The particularly distressing feature of these data are the large degradations of drag, even for a trailing distance of 9 calibers, and the lack of trend reversal to the highest test Mach number in this series. Although previous test data[5,7] suggested reasonable levels of supersonic drag to be imminent, those results were not obtained with the parachute trailing in the wake of the Viking forebody as in the present test series; the predicted supersonic results were therefore categorized as uncertain. It was quite evident that the canopy trailing distance should be increased to a value near $x/d = 9.0$, because the subsonic drag coefficient level increased from that experienced at lower x/d and the rate of transonic drag degradation was both substantially decreased and delayed to a higher Mach number.

Wind-Tunnel Tests (AEDC/PWT 16T and 16S Series)

The detailed plans[13,14] for this test series were made on the basis of the former series results at the 16-ft Transonic Dynamics Tunnel and projected parachute design changes having minimal impact on the Viking program in terms of both cost and schedule. As an example, increases in canopy trailing distance can be achieved by either introducing a riser line length between bridle and suspension-line confluence points or lengthening the parachute suspension-lines. Tradeoff studies indicated that lengthening the suspension lines was the preferable approach and, therefore, the test plans accentuated increasing S/D_o to reflect x/d increases to a maximum of about 11 forebody diameters to conform to parachute packaging density and mortar size constraints.

Figure 7 summarizes the test results in terms of parachute drag coefficient vs Mach number for five parachute configurations, reflecting simultaneous increase of x/d and S/D_o. Minimum drag is seen to occur at $M = 1.0$ for all tested configurations up to $x/d = 9.14$ and the corresponding S/D_o value of 1.85. The Mach number for minimum drag drops to 0.90 for the configuration positioned at $x/d = 11.02$. Also of interest is the reduced

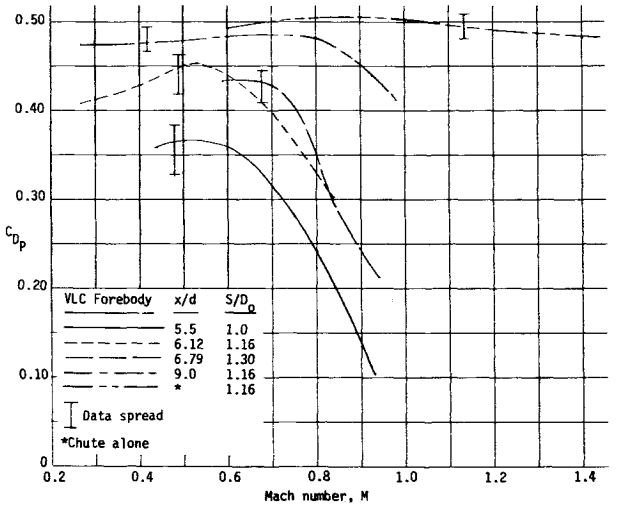

Fig. 6 Parachute drag coefficient vs Mach number (LRC).

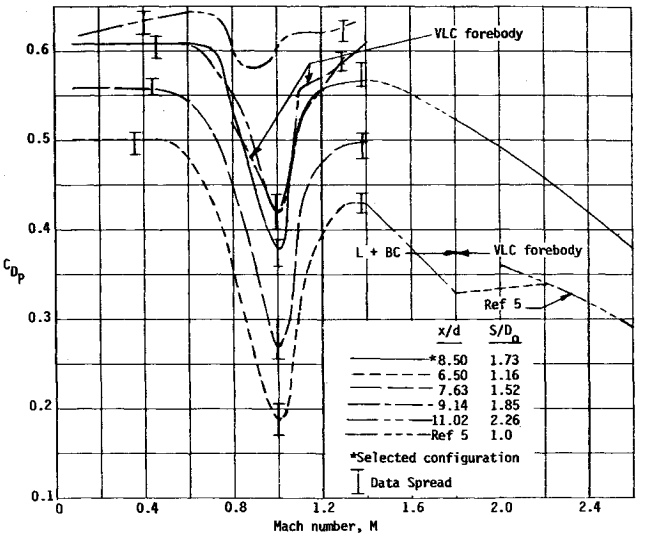

Fig. 7 Parachute drag coefficient vs Mach number (AEDC).

transonic drag reduction as trailing distance increases when compared to the subsonic drag coefficient value. What is unknown, however, is whether this trend primarily results from x/d or S/D_o increases. At a trailing distance of 8.5 forebody diameters and corresponding suspension line length ratio of $S/D_o = 1.73$, the drag curve as a function of Mach number very nearly represents the drag curve of the configuration represented by $x/d = 9.14$ and $S/D_o = 1.85$ within the uncertainty band. Accordingly, this configuration was selected as the redefined Viking baseline configuration. It should also be noted that the drag performance resulting from the selected configuration actually exceeded the original prediction. This benefit was accordingly reflected in increased allowable VLC entry weight.

Also shown in Fig. 7 is a parachute drag curve comparison at $x/d = 9.14$ and $S/D_o = 1.85$ in the wake of both VLC and L+BC forebodies. The differences are seen to be minor and are within the data uncertainty bands.

Parachute drag performance to $M = 2.6$ is shown only for the selected configuration represented by $x/d = 8.50$ and $S/D_o = 1.73$. It is seen that the transition from $M = 1.4$ to 1.8 (data gap) is smooth for the selected configuration but is abrupt for the former baseline configuration. Over the Mach range from 1.8 to 2.2, the drag remains almost constant for the closer trailing parachute, whereas the Ref. 5 curve more nearly represents the shape for the selected configuration. The drag coefficient magnitudes are similar when comparing the Ref. 5 curve with the closest trailing parachute configuration. The test arrangement for the reference investigations did not truly reflect parachute tests in a comparable wake. Accordingly, it is probable that the results are analogous to parachute tests at greater trailing distance and, therefore, the curve shape as a function of Mach number more nearly duplicates that experienced in this test series at greater trailing distances.

Suspension-Line Length Effects

Minimal data were obtained over the test Mach number range to directly determine the effects of increasing suspension-line length. Figure 8 presents all the data obtained and includes one comparison with the parachute trailing in the VLC forebody wake and some data obtained in the absence of the forebody. The dashed lines represent the effects of an S/D_o change from a value of 1.16 to 1.85 at a trailing distance behind the VLC forebody of $x/d = 9.14$. With the exception of a small Mach number range near 1.0, the configuration with increased suspension-line length provides for approximately 10% drag increases at $M = 0.8$ and substantially larger increases to almost

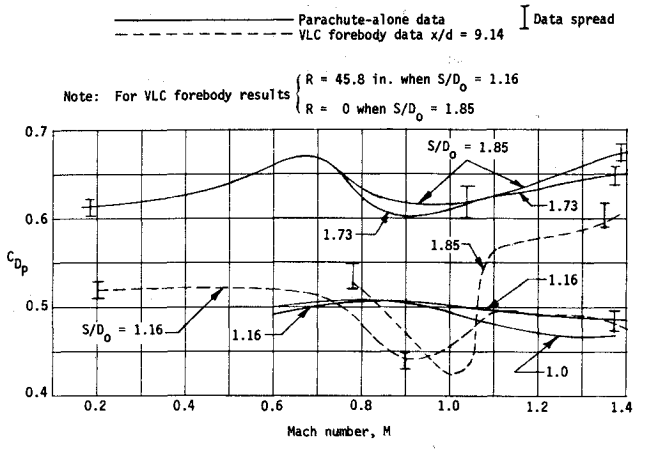

Fig. 8 Parachute drag coefficient vs Mach number at several values of S/D_o.

25% at $M \approx 1.4$. The corresponding parachute-alone drag coefficient values for $S/D_o = 1.16$ are equivalent (within data spread) to those measured for the configuration trailing the VLC forebody, with the exception of the drag bucket between $M = 0.75$ and 1.10. Comparison of data for parachute-alone tests also reveals increases of 20% or more in parachute drag coefficient over the entire test Mach number range when increasing S/D_o from about 1.0 to 1.73. It is perhaps noteworthy that S/D_o increases beyond 1.73 (selected configuration) might further increase the parachute drag coefficient at $M > 1.4$, as indicated by the divergent trend of the curves in Fig. 8.

Selected Configuration Performance

In Fig. 9, performance of the selected parachute configuration from the wind-tunnel tests is compared with results obtained during an Earth atmosphere flight test.[15,16] The results of the parachute-alone wind-tunnel tests are also included in this figure. The flight hardware qualification test program consisted of a simulation of predicted environmental conditions at parachute deployment and obtaining parachute performance from the flown trajectory after mortar firing. Conditions at mortar firing for the AV-4 flight[16] represent a Mach number of 2.13 and dynamic pressure $q_\infty = 10.9$ lb/ft^2. Subsequent parachute drag performance is also shown in Fig. 9. It is seen that the wind-tunnel data compare well (within $\pm 5\%$) with the flight test data from low subsonic Mach numbers to about $M = 1.0$. Beyond this Mach number, the differences become greater, with the wind-tunnel data under-predicting the flight results. The reason for this disagreement is not known, although it is possible that the relatively stiffer 10% scale-model parachute could not stretch and deform to the degree actually experienced by the flight article. The deformation would naturally be more effective at the higher dynamic pressures (supersonically) than at the lower flight-test Mach numbers, which can in part account for some portion of the difference. In addition, the flight test represents a rapid supersonic deceleration of the combined forebody and decelerator system unlike the specific steady-state test condition represented by wind-tunnel tests. It is possible that forebody wake differences contrasting a rapid deceleration with a steady-state wake also account for the differences between wind-tunnel and flight tests in the supersonic test regime.

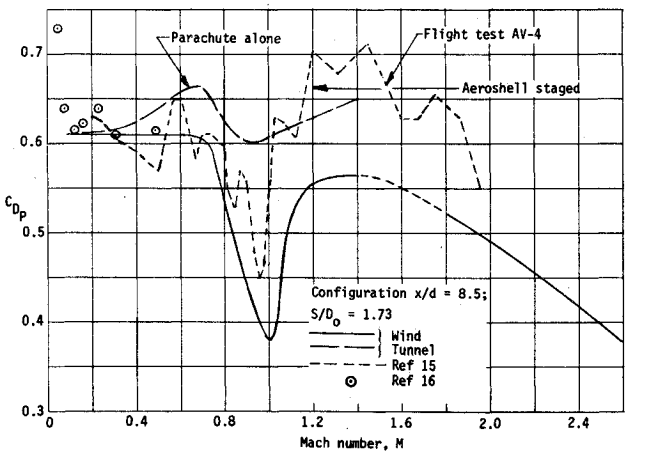

Fig. 9 Comparison of wind-tunnel and flight-test parachute performance.

Conclusions

A series of wind-tunnel investigations to obtain the drag performance of 10% scale disk-gap-band parachute assembly configurations trailing in the Viking forebody wake were conducted over a Mach number range from 0.2 to 2.6 at AEDC PWT and NASA Langley Research Center 16-ft tunnel facilities. The tests involved variation of both parachute trailing distance and suspension-line length to optimize both parachute assembly position and configuration; the tests also involved parachute-alone performance. In addition, some water-table investigations, using two-dimensional models of forebody and parachute canopy, were made to qualitatively assess the flowfield of the mutually interfering bodies. The test results provided the following major conclusions:

1) Parachute drag performance in the forebody wake is markedly degraded, beginning at $M \approx 0.6$, and reaches a minimum value at sonic speed; the reductions are as much as 60% below the corresponding value at $M \approx 0.6$.

2) More than a 20% increase in drag performance over the entire Mach number range is realized when increasing trailing distance from 6.5 to 8.5 forebody diameters by lengthening the suspension lines; this method for obtaining increased drag performance is more effective than providing an equivalent riser line length.

3) The transonic drag coefficient for the parachute alone is increased by 20% by increasing S/D_o from 1.16 to 1.73.

4) Flight-test and wind-tunnel data are in good agreement, particularly at Mach numbers < 1.0.

5) Qualitative photographic evidence (water table) substantiates increased parachute drag performance with increases in canopy trailing distance from 5 to 8 forebody diameters.

References

[1] "Mars Engineering Model," M75-125-1, Dec. 1970, NASA.

[2] Murrow, H. N. and McFall, J. C., Jr., "Some Test Results from the NASA Planetary Entry Parachute Program," *Journal of Spacecraft and Rockets*, Vol. 6, No. 5, May 1969, pp. 621–623.

[3] Whitlock, C. H. and Bendura, R. J., "Inflation and Performance of Three Parachute Configurations from Supersonic Flight Tests in a Low-Density Environment," TND-5296, July 1969, NASA.

[4] Eckstron, C. V. and Murrow, H. N., "Flight Tests of Cross, Modified Ringsail, and Disk-Gap-Band Parachutes from a Deployment Altitude of 3.05 km (10,000 ft)," TM X-2221, June 1971, NASA.

[5] Bobbitt, P. J., Mayhue, R. J., Faurote, G. L., and Galigher, L. L., "Supersonic and Subsonic Wind-Tunnel Tests of Reefed and Unreefed Disk-Gap-Band Parachutes," AIAA Paper 70-1172, Wright-Patterson Air Force Base, Ohio, 1970.

[6] Galigher, L. L., "Aerodynamic Characteristics of Ballutes and Disk-Gap-Band Parachutes at Mach Numbers from 1.8 to 3.7," AEDC TR-69-245, Nov. 1969, ARO, Inc., Arnold Air Force Station, Tenn.

[7] Mayhue, R. J. and Bobbitt, P. J., "Drag Characteristics of a Disk-Gap-Band Parachute with a Nominal Diameter of 1.65 Meters at Mach Numbers of 2.0 to 3.0," TN D-6894, Oct. 1972, NASA.

[8] Jaremenko, I., Steinberg, S., and Faye-Petersen, R., "Scale Model Test Results of the Viking Parachute System at Mach Numbers from 0.1 through 2.6," TR-3720181, Nov. 1971, Martin Marietta Corp., Denver, Colo.

[9] Reichenau, D. E. A., "Aerodynamic Characteristics of Disk-Gap-

Band Parachutes in the Wake of Viking Entry Forebodies at Mach Numbers from 0.2 to 2.6," AEDC-TR-72-78, July 1972, ARO, Inc., Arnold Air Force Station, Tenn.

[10] "Propulsion Wind Tunnel Facility," *Test Facilities Handbook*, 9th ed., Vol. 4, Arnold Engineering Development Center, Tullahoma, Tenn., July 1971.

[11] "The Langley Transonic Dynamics Tunnel," Langley Working Paper LWP-799, Sept. 23, 1969, NASA.

[12] Steinberg, S. and Faye-Petersen, R., "Pre-Test Report for Flexible Decelerator Wind Tunnel Tests at AEDC PWT," TP-3720060, Jan. 1971, Martin Marietta Corp., Denver, Colo.

[13] Steinberg, S., "Pre-Test Report for Flexible Decelerator Wind Tunnel Tests at AEDC PWT 16T (Phase 2)," TP-3720157, June 1971, Martin Marietta Corp., Denver, Colo.

[14] Jaremenko, I., "Pre-Test Report for Flexible Decelerator Wind Tunnel Tests at AEDC PWT 16S," TP-3720168, July 1971, Martin Marietta Corp., Denver, Colo.

[15] Moog, R. D. and Michel, F. C., "Balloon Launched Viking Decelerator Test Program Summary Report," TR-3720359, March 1973, Martin Marietta Corp., Denver, Colo.

[16] Dickinson, D., Schlemmer, J. W., Hicks, F., Michel, F. C., and Moog, R. D., "Balloon Launched Decelerator Test Program; Post-Flight Test Report, BLDT Vehicle AV-4," TR-3720295, Oct. 1972, Martin Marietta Corp., Denver, Colo.

FEBRUARY 1974 J. SPACECRAFT VOL. 11, NO. 2

Skylab Experience with Apollo Docking/Latching Loads

R. A. HEATH*
Martin Marietta Aerospace, Denver Division
AND
W. B. HOLLAND†
NASA Marshall Space Flight Center, Huntsville, Ala.

Since the early development stages of Apollo, the docking probe mechanism has confronted the structural dynamicist with a modeling and structural response challenge. Skylab is an excellent example of a structure where complexity of analytical models and subsequent dynamic analysis is fully justified. This paper describes the four-year development of Skylab analytical programs, mathematical model complexity, and vibration and load analyses associated with the docking/latching maneuver. Examples are shown where coarse models produced loads in excess of structural capability. However, subsequent model refinement lowered the loads to the point where redesign was not required. A summary of experience gained over a four-year period is presented in the conclusions.

I. Introduction

SKYLAB is a 100-ton manned orbital scientific space station designed to accomplish scientific and technical experiments and medical investigations while in near-earth orbit. The primary source of power for Skylab is provided by large flexible solar array systems (SAS) which require special handling to prevent panel buckling or other structural damage under their own weight.

The transient loading conditions, occurring during the atmospheric boost phase of flight, design the primary structural elements of Skylab with the exception of the docking interfaces, solar arrays, and deployment structure. The orbital vacuum environment causes no external forces on the vehicle. The orbital events considered in the design of Skylab are docking, latching, orbit maneuvers, and the several deployment sequences. Since docking and latching are the significant load-producing events, this paper will be limited to the discussion of these two events.

In the early design stages of Skylab, an acceleration value of 0.2 g was used to simulate the loads due to the orbital docking and latching event. This was adequate for preliminary design, but changed considerably as the design progressed. Docking and latching forcing functions were derived and used to calculate the response loads at selected coordinates. This process became more complicated as the models grew in sophistication.

This paper describes the evolution of the Skylab models and the vibration analyses performed in support of the docking and latching event. In addition, the paper lists criteria derived from Skylab experience and considered applicable for future orbital space station development.

II. Configurations

The Skylab orbital cluster consists of the Orbital Workshop (OWS), Instrument Unit (IU), Fixed Airlock Shroud (FAS), Airlock Module (AM), Structural Transition Section (STS), DA truss, Multiple Docking Adapter (MDA), deployed ATM, and deployed SASs of the ATM and OWS. When the Command and Service Module (CSM) docks to the axial port of the MDA, this configuration (Fig. 1) is called Axial Configuration. The rescue mission requires the use of another CSM docked to the MDA radial port; this is referred to as Radial Configuration. These are the configurations used to perform the vibration and loads analyses which follow.

III. Skylab Vibration Analyses Chronology

In early 1969, mathematical models were represented primarily with equivalent beam stiffnesses. This "stick" model consisted of a mass spring representation of the modules which make up the configuration of Fig. 1. Only the ATM rack structural model is

Presented as Paper 73-613 at the AIAA/ASME/SAE Joint Space Mission Planning and Execution Meeting, Denver, Colo., July 10–12, 1973; submitted July 20, 1973; revision received October 1, 1973.

Index category: Structural Dynamic Analysis.

* Group Engineer—Skylab Dynamics. Member AIAA.

† Dynamics Engineer.